Supplementary Information for

Harnessing Non-Uniform Pressure Distributions: The Next Generation of Soft Robotic Actuators

Yoav Matia†, Gregory H. Kaiser,
Robert F. Shepherd, Amir D. Gat, Nathan Lazarus, and Kirstin H. Petersen

†To whom correspondence should be addressed; E-mail: ym279@cornell.edu

This PDF file includes:

Supplementary text
Table A.1.
Figs. B.1. to B.5.
Table B.1. , B.2.
Figs. C.1 , C.2.

Other supplementary materials for this manuscript include the following:
Movies 1 to 6

Contents

†E-mail: ym279@cornell.edu

Appendix A

Q	Ref.	Robot Archtype	Untethered	Dynamic Predictive Model	Fluid	Dynamic viscosity, μ [Pa·s]	Change in Cross Section per Pressure, $(\partial a_1/\partial p)\|_{p=p_0}$ $[m^2/\text{Pa}]$	Characteristic Fluidic Cross Section, a_0^* $[m^2]$	Fluid Domain Slenderness, $\epsilon_1=l_{\text{eff}}/l$	Mass per Unit Length, m[kg/m]
1.	14.	Appendage	Y	Y	60:40 Glycerin–Water	$1.\times10^{-2}$	1.76×10^{-10}	3.14×10^{-6}	0.011	1.050
1.	27.	Tripodal	N	N	Combustion	1.8×10^{-5}	1.87×10^{-12}	1.87×10^{-5}	0.062	0.064
1.	28.	Appendage	N	N	Air	1.8×10^{-5}	1.11×10^{-9}	1.13×10^{-4}	0.075	0.578
1.	29.	Appendage	N	Y	Air	1.8×10^{-5}	1.58×10^{-12}	$4.\times10^{-6}$	0.002	1.230
1.	30.	Hand Apparatus	N	N	Air	1.8×10^{-5}	8.18×10^{-12}	1.8×10^{-5}	0.063	0.202
1.	31.	Appendage	N	Y	Air	1.8×10^{-5}	8.75×10^{-11}	$4.\times10^{-6}$	0.001	1.200
1.	31.	Appendage	N	Y	Water	$1.\times10^{-3}$	8.75×10^{-11}	$4.\times10^{-6}$	0.001	1.200
2.	13.	Appendage	N	Y	Silicone Oil	5.82×10^{1}	8.75×10^{-11}	$4.\times10^{-6}$	0.001	1.200
2.	13.	Appendage	N	Y	85:15 Glycerin–Water	1.15	8.75×10^{-11}	$4.\times10^{-6}$	0.001	1.200
2.	15.	Legged Hexapod	N	N	Air	1.8×10^{5}	5.63×10^{-10}	2.56×10^{-4}	0.320	2.560
2.	16.	Appendage	N	Y	60:40 Glycerin–Water	$1.\times10^{-2}$	2.86×10^{-8}	3.14×10^{-6}	0.001	0.454
2.	31.	Appendage	N	Y	Glycerin	1.15	8.75×10^{-11}	$4.\times10^{-6}$	0.001	1.200
3.	This Study	Legged Hexapod	Y	Y	Air	1.8×10^{-5}	3.41×10^{-9}	3.32×10^{-7}	0.001	0.269
3.	This Study	Legged Hexapod	Y	Y	Water	$1.\times10^{-2}$	3.41×10^{-9}	3.32×10^{-7}	0.001	0.269
4.	12.	legged quadruped	Y	N	CO2	1.8×10^{-5}	7.32×10^{-10}	1.02×10^{-3}	0.208	0.152
4.	17.	Legged Quadruped	N	Y	Air	1.8×10^{-5}	$4.\times10^{-9}$	1.2×10^{-4}	0.100	0.668
4.	18.	Legged Octopod	Y	N	Mono–propellant	1.8×10^{-5}	5.46×10^{-12}	1.96×10^{-7}	0.020	0.062
4.	19.	Legged Quadruped	Y	N	CO2	1.8×10^{-5}	1.41×10^{-10}	1.96×10^{-5}	0.023	1.910
4.	20.	Swimming Robot	N	N	Air	1.8×10^{-5}	1.57×10^{-10}	1.57×10^{-4}	0.063	0.117
4.	21.	24 Legged Robot	N	N	Air	1.8×10^{-5}	7.96×10^{-10}	2.68×10^{-4}	0.133	0.300
4.	22.	Appendage	N	Y	Air	1.8×10^{-5}	2.24×10^{-10}	1.51×10^{-4}	0.109	0.169
4.	23.	Legged Quadruped	N	N	Air	1.8×10^{-5}	6.22×10^{-11}	3.14×10^{-6}	0.022	0.115
4.	24.	Appendage	N	N	Nitrogen	1.85×10^{-5}	1.45×10^{-10}	3.72×10^{-5}	0.071	0.265
4.	25.	Legged Quadpod	N	N	Water Based MR Fluid	6.25×10^{-2}	3.33×10^{-9}	$3.\times10^{-5}$	0.050	0.065
4.	26.	Appendage	N	N	Air	1.8×10^{-5}	6.03×10^{-11}	4.02×10^{-6}	0.005	0.004

TABLE. A.1. ***Characterization of the state-of-the-art in soft robotics[1,2], used in figure 1.*** *Tabulated data, Columns 1-11 out of 20.*

[1] Data presented herein is based on information reported or derived implicitly via images and figures when no such information was provided explicitly. Accordingly, some data may vary by a factor. However, great care was taken to ensure that the critical parameters associated with a given system are identified to properly position it in the correct quadrant.

[2] In the absence of any references to actual actuation times in an article, care was taken to pick a value that was matched by the system's own timescales in order to position the work in the right quadrant in line with the authors' report of the transient regime (quasistatic or inertial).

Q	Ref.	Appendage Length, l_z [m]	Young Modulus, E[Pa]	AVG. Moment of Inertia, I $[m^4]$	Stiffness Correction Coefficient, f_i	Viscous–Elastic Time Scale, t_f^* [s]	Inertial–Elastic Time Scale, t_z^* [s]	Input Time Scale, t_i^* [s]	Plot x–axis	Plot y–axis
1.	14.	0.100	$2.\times10^{6}$	3.86×10^{-8}	0.600	0.005	0.048	0.031	1.05×10^{1}	1.53
1.	27.	0.075	$4.\times10^{4}$	$5.\times10^{-10}$	0.600	4.630×10^{-10}	0.411	0.050	8.88×10^{8}	8.23
1.	28.	0.100	$4.\times10^{4}$	1.46×10^{-11}	0.300	3.170×10^{-8}	18.200	1.000	5.74×10^{8}	1.82×10^{1}
1.	29.	0.100	$8.\times10^{5}$	1.43×10^{-9}	0.800	1.690×10^{-6}	0.116	0.004	6.85×10^{4}	2.89×10^{1}
1.	30.	0.130	$4.\times10^{4}$	1.28×10^{-9}	0.500	2.050×10^{-9}	1.500	1.000	7.34×10^{8}	1.5
1.	31.	0.200	1.5×10^{6}	1.3×10^{-8}	0.800	0.000	0.351	0.083	1.39×10^{3}	4.21
1.	31.	0.200	1.5×10^{6}	1.3×10^{-8}	0.800	0.014	0.351	0.083	2.51×10^{1}	4.21
2.	13.	0.200	1.5×10^{6}	1.3×10^{-8}	0.800	815.000	0.351	0.003	4.31×10^{-4}	1.4×10^{2}
2.	13.	0.200	1.5×10^{6}	1.3×10^{-8}	0.800	16.100	0.351	0.003	2.18×10^{-2}	1.4×10^{2}
2.	15.	0.050	1.98×10^{4}	5.46×10^{-9}	0.505	3.860	0.542	0.325	1.4×10^{-1}	1.67
2.	16.	0.125	9.7×10^{5}	2.73×10^{-9}	0.900	41.400	0.215	0.083	5.2×10^{-3}	2.58
2.	31.	0.200	1.5×10^{6}	1.3×10^{-8}	0.800	16.100	0.351	0.083	2.18×10^{-2}	4.21
3.	This Study	0.109	1.8×10^{6}	4.5×10^{-8}	0.550	0.158	0.029	0.875	1.85×10^{-1}	3.34×10^{-2}
3.	This Study	0.109	1.8×10^{6}	4.5×10^{-8}	0.550	87.700	0.029	5.000	3.33×10^{-4}	5.84×10^{-3}
4.	12.	0.173	2.7×10^{9}	1.69×10^{-8}	1.000	2.990×10^{-10}	0.002	1.320	5.78×10^{6}	1.31×10^{-3}
4.	17.	0.075	$4.\times10^{4}$	1.98×10^{-8}	0.500	6.000×10^{-8}	0.231	4.550	3.85×10^{6}	5.08×10^{-2}
4.	18.	0.032	1.5×10^{4}	$4.\times10^{-12}$	0.800	1.250×10^{-6}	1.160	10.900	9.28×10^{5}	1.07×10^{-1}
4.	19.	0.216	$7.\times10^{6}$	2.21×10^{-6}	0.500	2.420×10^{-7}	0.023	0.500	9.58×10^{4}	4.63×10^{-2}
4.	20.	0.080	9.7×10^{5}	3.51×10^{-10}	1.000	4.610×10^{-9}	0.119	0.200	2.58×10^{7}	5.94×10^{-1}
4.	21.	0.060	$1.\times10^{6}$	1.68×10^{-9}	1.000	3.010×10^{-9}	0.048	0.200	1.6×10^{7}	2.41×10^{-1}
4.	22.	0.055	$1.\times10^{6}$	6.51×10^{-10}	1.000	2.250×10^{-9}	0.049	0.200	2.17×10^{7}	2.44×10^{-1}
4.	23.	0.045	$4.\times10^{4}$	3.54×10^{-10}	0.500	7.220×10^{-7}	0.258	1.000	3.57×10^{5}	2.58×10^{-1}
4.	24.	0.086	$7.\times10^{6}$	2.41×10^{-9}	0.500	1.430×10^{-8}	0.041	0.050	2.9×10^{6}	8.29×10^{-1}
4.	25.	0.040	$8.\times10^{5}$	4.5×10^{-11}	0.900	0.003	0.072	10.000	2.58×10^{1}	7.16×10^{-3}
4.	26.	0.320	5.16×10^{5}	2.32×10^{-12}	0.500	0.000	8.400	84.000	7.78×10^{5}	$1.\times10^{-1}$

[1] Data presented herein is based on information reported or derived implicitly via images and figures when no such information was provided explicitly. Accordingly, some data may vary by a factor. However, great care was taken to ensure that the critical parameters associated with a given system are identified to properly position it in the correct quadrant.

[2] In the absence of any references to actual actuation times in an article, care was taken to pick a value that was matched by the system's own timescales in order to position the work in the right quadrant in line with the authors' report of the transient regime (quasistatic or inertial).

TABLE. A.1. ***Characterization of the state-of-the-art in soft robotics[1,2], used in figure 1****. Tabulated data, Columns 12-20 out of 20.*

Appendix B

B.1. Nomenclature

We define vector variables by bold letters, direction vectors by hat notation, non-dimensional variables by tilde or capital letters and characteristic values by asterisk superscripts.

System physical parameters

l_s	Beam length.
h_s	Beam height.
w_s	Beam width.
E	Beam material modulus of elasticity.
ρ_s	Beam material mass density.
f_m	Solid mass fraction.
f_e	Cross sectional extensional stiffness correction coefficient, comparing the honeycomb structure to a full rectangular cross section structure with identical dimensions.
f_i	Cross sectional flexural stiffness correction coefficient, comparing the honeycomb structure to a full rectangular cross section structure with identical dimensions.
m	Beam mass per unit length.
I	Beam cross section moment of inertia.
y^{11}, Y^{11}	Gyration radius squared, and its non-dimensional form.
ψ	Change in beam slope due to a single pressurized bladder (intrinsically non-dimensional).
$\zeta, \tilde{\zeta}$	Change in beam length due to a single pressurized bladder, and its non-dimensional form.
ϕ, Φ	Structure length-wise bladder density, and its non-dimensional form.
l_b	Length of a single bladder segment.
h_b	Height of a fluidic bladder cross section.
w_b	Width of a fluidic bladder cross section.
n	Total number of bladder (fluidic cavities) in the honeycomb structure.
ρ_f	Fluid domain material mass density.
μ	Fluid dynamic viscosity.
ε_1	Small parameter representing slenderness of the fluidic domain.
r_c	Connective tubing radius.
l	Total length of connective tubing configuration.
l_c	Length of a single connective tube.
n_c	Total number of connective tubes in a given configuration.
σ_p	Ratio of a_0^* the characteristic cross-section at gage pressure to a_1^* the characteristic change in bladder cross-section.
r_{eff}	Effective dimensional scale related to the configuration of the flow-path i.e. averaged hydraulic radii of bladder and connective tubing.
$\tilde{C}^b$	Dimensionless constant, related to the bladder flow-path i.e. shape of the bladder cross-section.
$\tilde{C}^c$	Dimensionless constant, related to the connective tubing flow-path i.e. shape of connective tube cross-section.

Variables and arguments

t, T, T_s	Time dimension, viscous-elastic non-dimensional time, and Inertial-elastic non-dimensional time.
θ, Θ	Curvilinear length coordinate along the beam reference curve, and its non-dimensional form.
$(\hat{\boldsymbol{x}}_{\boldsymbol{s}}, \hat{\boldsymbol{y}}_{\boldsymbol{s}}, \hat{\boldsymbol{z}}_{\boldsymbol{s}})$	Solid domain lab frame of reference.
(x_s, y_s, z_s) , (X_s, Y_s, Z_s)	Solid domain lab frame coordinates, and their non-dimensional form.
$\boldsymbol{x}$	Lab frame position vector for the beam reference curve (i.e. the neutral axis).
$({}^{s}\boldsymbol{e_n}, {}^{s}\boldsymbol{e_\tau}, {}^{s}\boldsymbol{e_t})$, $({}^{s}\boldsymbol{E_n}, {}^{s}\boldsymbol{E_\tau}, {}^{s}\boldsymbol{E_t})$	Spatial Serret-Ferent triad (at time t) associated with the current position along the reference curve in a curvilinear frame using the unit tangent ${}^{s}\boldsymbol{e}_t$ pointing the direction of motion, the unit normal ${}^{s}\boldsymbol{e}_n$, unit binormal ${}^{s}\boldsymbol{e}_\tau$, and their non-dimensional form.
$(\boldsymbol{d_1}, \boldsymbol{d_2}, \boldsymbol{d_3})$	Spatial director (strain vector at time t), in the curvilinear frame of reference $({}^{s}\boldsymbol{e_n}, {}^{s}\boldsymbol{e_\tau}, {}^{s}\boldsymbol{e_t})$.
$(\boldsymbol{D_1}, \boldsymbol{D_2}, \boldsymbol{D_3})$	Material director (strain vector at time $t = 0$), in the curvilinear frame of reference $({}^{s}\boldsymbol{e_n}, {}^{s}\boldsymbol{e_\tau}, {}^{s}\boldsymbol{e_t})$.
u_1, U_1	Beam deflection displacement and its non-dimensional form.
u_3, U_3	Beam extension displacement and its non-dimensional form.
$\lambda_s, \tilde{\lambda}_s$	Total structure measure of stretch, Intrinsic kinematic variable, and its non-dimensional form.
$\lambda_e, \tilde{\lambda}_e$	Measure of stretch due to external traction, Intrinsic kinematic variable, and its non-dimensional form.
$\lambda_p, \tilde{\lambda}_p$	Measure of stretch due to fluidic pressure, Intrinsic kinematic variable, and its non-dimensional form.
$\alpha_s, \tilde{\alpha}_s$	Total structure measure of curvature, Intrinsic kinematic variable, and its non-dimensional form.
$\alpha_e, \tilde{\alpha}_e$	Measure of curvature due to external traction, Intrinsic kinematic variable, and its non-dimensional form.
$\alpha_p, \tilde{\alpha}_p$	Measure of curvature due to fluidic pressure, Intrinsic kinematic variable, and its non-dimensional form.
$N_e, \tilde{N}_e$	Cross sectional internal normal force resultant due to traction, and its non-dimensional form.
$V_e, \tilde{V}_e$	Cross sectional internal shear force resultant due to traction, and its non-dimensional form.
$M_e, \tilde{M}_e$	Cross sectional internal moment resultant due to traction, and its non-dimensional form.
$\boldsymbol{d^3}$	The reciprocal vector to $\boldsymbol{d}_3$.
$\boldsymbol{b}, \boldsymbol{B}$	External distributed force per unit mass.
$\boldsymbol{b^1}, \boldsymbol{B^1}$	External distributed moment per unit mass.
$\boldsymbol{b_b}, \boldsymbol{B_b}$	Body force distribution per unit mass, and its non-dimensional form.
$\boldsymbol{b_c}, \boldsymbol{B_c}$	Contact force distribution per unit mass, and its non-dimensional form.
$\boldsymbol{b_b^1}, \boldsymbol{B_b^1}$	First moment of body force distribution per unit mass, and its non-dimensional form.
$\boldsymbol{b_c^1}, \boldsymbol{B_c^1}$	First moment of contact force distribution per unit mass, and its non-dimensional form.

$(\hat{\boldsymbol{x}}_{\boldsymbol{f}}, \hat{\boldsymbol{y}}_{\boldsymbol{f}}, \hat{\boldsymbol{z}}_{\boldsymbol{f}})$	Fluidic domain curvilinear frame of reference. Defined such that the $\hat{\boldsymbol{x}}_f$ is the streamwise direction along bladder length l_b, and the cross sectional plane $\hat{\boldsymbol{y}}_f - \hat{\boldsymbol{z}}_f$ is perpendicular to $\hat{\boldsymbol{x}}_f$.
(x_f, y_f, z_f) , (X_f, Y_f, Z_f)	Fluid domain curvilinear coordinates, and their non-dimensional form.
(u, v, w) , (U, V, W)	Fluid domain velocity components, and their non-dimensional form.
p, P	Fluid domain pressure, and its non-dimensional form.
p', P'	Bladder effective fluid pressure for slope generation, and its non-dimensional form.
$\bar{p}, \bar{P}$	Bladder effective fluid pressure for extension generation, and its non-dimensional form.
q, Q	Volume flow rate in fluidic cross section, and its non-dimensional form.
q_1^b, Q_1^b	Bladder permeability, and its non-dimensional form.
q_1^c, Q_1^c	Connective tubes' permeability, and its non-dimensional form.
a, A	Fluid domain cross section area, and its non-dimensional form.
a_0, A_0	Cross section area of the bladder-tube array at gauge pressure $p = 0$, and its non-dimensional form.
a_{p_1}, A_{p_1}	The change of the cross section area due to the fluid pressure, and its non-dimensional form.
a_{N_1}, A_{N_1}	The change in cross section are due to extensional beam deformation, and its non-dimensional form.
a_{M_1}, A_{M_1}	The change in cross section due to beam bending deformation, and its non-dimensional form.

Characteristic Scales

u_1^*	Characteristic beam deflection.
u_3^*	Characteristic beam extension.
b_b^{1*}	Characteristic first moment of body force distribution per unit mass.
b_c^{1*}	Characteristic first moment of contact force distribution per unit mass.
b_b^*	Characteristic body force distribution per unit mass.
b_c^*	Characteristic contact force distribution per unit mass.
b_x^*	Characteristic shear force per unit length.
b_z^*	Characteristic normal force per unit length.
b^*	Characteristic external force per unit mass.
b^{1*}	Characteristic external moment applied per unit mass.
b_x^{1*}	Characteristic first moment applied by shear force $(x - axis)$ per unit length.
b_z^{1*}	Characteristic first moment applied by normal force $(z - axis)$ per unit length.
ϕ^*	Characteristic bladder density.
t_s^*	Elastic-inertial time scale.
α_s^*	Characteristic curvature.
M_e^*	Characteristic moment resultant.
y_{11}^*	Characteristic squared radius of gyration.
(u^*, v^*, w^*)	Characteristic fluid velocity.
a_0^*	Characteristic cross-section at gage pressure.
a_1^*	Characteristic change in bladder cross-section.

t_f^*	Viscous-elastic time scale.
u^*	Characteristic axial flow velocity.
p^*	Characteristic fluid pressure.

TABLE. A.1. ***Summary of Nomenclature for proposed model. Entries are by order of appearance.*** *(a) system physical parameters. (b) Variable and arguments. (c) Characteristic scales. Calculated entries are referred to respective sections.*

B.2. Problem Formulation

We consider the dynamics of an elastic beam, initially at rest. The internal structure of the beam is a fluid filled bladder matrix interconnected by slender tubing (as illustrated in Fig. B.1.). Pressure within the fluid field both generates and is induced by the deformation of the appendage (interchangeably referred to as leg). Note: bladders in this appendix are referred to as top and bottom respective right and left in the main text due to system orientation in respective figure.

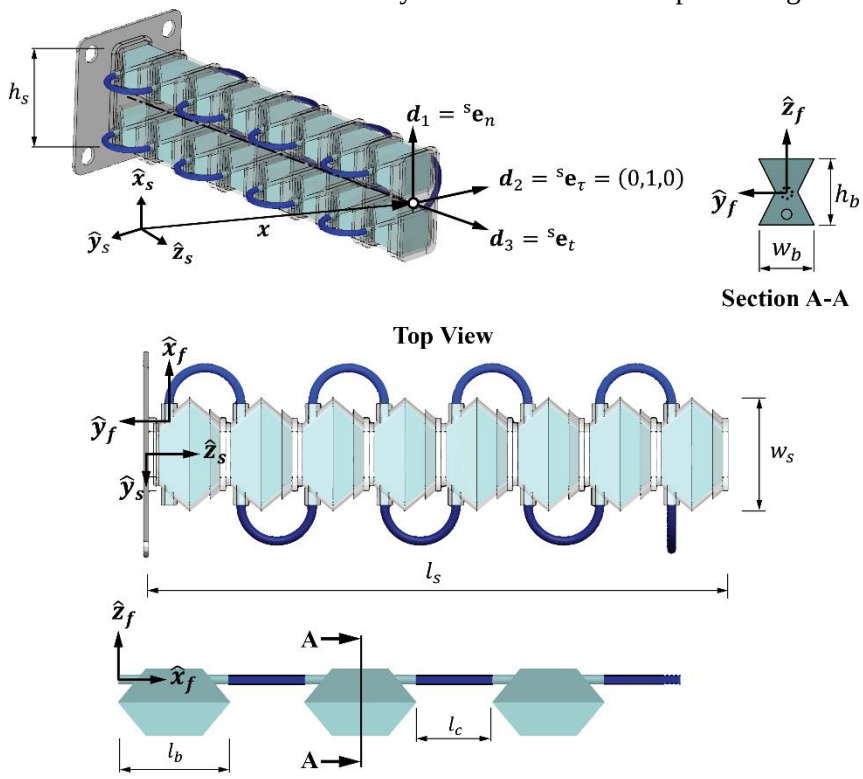

FIG. B.1. ***Illustration of the studied soft robotics appendage, with interconnected bladder-tube array configuration.***

We define vector variables by bold letters, direction vectors by hat notation, non-dimensional variables by tilde or capital letters and characteristic values by asterisk superscripts. We define appendage length l_s, height h_s, width w_s and require a slender geometry with $h_s/l_s \ll 1$ and $w_s/l_s \ll 1$. Appendage material modulus of elasticity and mass density are defined by E and ρ_s, respectively. We define a lab frame of reference $(\boldsymbol{e}_1, \boldsymbol{e}_2, \boldsymbol{e}_3) = (\hat{\boldsymbol{x}}_s, \hat{\boldsymbol{y}}_s, \hat{\boldsymbol{z}}_s)$ and a lab frame position vector $\boldsymbol{x} = (x_s(\theta,t), y_s(\theta,t),\ z_s(\theta,t))$ for the appendage reference curve (i.e. the neutral axis). We define the deformation of a material fiber in the cross section area in a curvilinear frame of reference using the strain vectors, denoted spatial directors $(\boldsymbol{d}_1(\theta,t), \boldsymbol{d}_2(\theta,t), \boldsymbol{d}_3(\theta,t))$ and respective material directors $(\boldsymbol{D}_1(\theta), \boldsymbol{D}_2(\theta), \boldsymbol{D}_3(\theta))$. We define a Serret-Ferent triad associated with the current position along the reference curve in a curvilinear frame using the unit tangent ${}^s\boldsymbol{e}_t$ pointing the direction of motion, the

unit normal ${}^{s}\boldsymbol{e}_n$, unit binormal ${}^{s}\boldsymbol{e}_\tau$, and define a curvilinear length coordinate θ along the beam reference curve (see Figs. B.1).

We limit our analysis to a 2D deformation thus considering only directors $(\boldsymbol{d}_1(\theta,t), \boldsymbol{d}_3(\theta,t))$. We thus redefine the lab frame position vector $\boldsymbol{x} = (x_s(\theta,t), z_s(\theta,t))$ with the deflection axis in the $\boldsymbol{e}_1$ direction being $x_s(\theta,t) = x_0(\theta) + u_1(\theta,t)$ and extension axis in the $\boldsymbol{e}_3$ direction $z_s(\theta,t) = z_0(\theta) + u_3(\theta,t)$ where for an appendage initially (at $t = 0$) straight at unstrained state, $x_0(\theta) = Const, z_0(\theta) = \theta$, and thus $x_s(\theta,t) = Const + u_1(\theta,t)$ and $z_s(\theta,t) = \theta + u_3(\theta,t)$ respectively.

The explicit representations of relevant directors are,

$$\boldsymbol{d}_1 = \left(\frac{\partial z_s}{\partial \theta}, -\frac{\partial x_s}{\partial \theta}\right), \tag{B.1}$$

$$\boldsymbol{d}_3 = \left(\frac{\partial x_s}{\partial \theta}, \frac{\partial z_s}{\partial \theta}\right). \tag{B.2}$$

A parallel bladders' matrix is interconnected and arranged perpendicular to the $\boldsymbol{d}_3$ direction along the appendage length. The length of a single bladder segment is denoted l_b. The effect of the fluidic cavities on structure properties are represented by the solid mass fraction $f_m = ((w_b h_b l_b n)\rho_f + (l_s w_s h_s - w_b h_b l_b n)\rho_s)/(l_s w_s h_s \rho_s)$, mass per unit length $m = \rho_s(w_s h_s) f_m$, coefficients f_e, f_i correct for cross section extensional and flexural stiffness reduction compared with a full elastic beam, appendage cross section moment of inertia $I = (w_s h_s^3/12) f_i$ and the squared gyration radius $y^{11} = (\rho_s/m)I$. We limit our analysis to configurations where the bladders are taken as unit-cells of the structure $w_b/l_s \ll 1$ and $(w_b \cdot n/2)/l_s \sim 1$, where $n/2$ is the total number of bladders arranged along the length l_s; enabling us in order to approximate the above structural properties to constants representing an averaged property of the solid domain.

Constitutive laws are formulated using the intrinsic kinematic variables of λ for the measure of stretch and α for curvature. The total stretch is defined by $\lambda_s = \lambda_e + \lambda_p$ and total curvature is defined by $\alpha_s = \alpha_e + \alpha_p$. Both λ_e and α_e are due to external traction and λ_p, α_p are due to pressure in the fluidic cavities. We define the cross-sectional internal forces and moment resultants due to traction for normal force N_e, shear force V_e and moment M_e. A single pressurized bladder will create a change in beam slope ψ and a change in beam length defined ζ, and structure bladder density $\phi = (n/2)/l_s$.

We introduce a fluidic domain coordinate system (x_f, y_f, z_f) defined such that the $\hat{\boldsymbol{x}}_f$ is the streamwise direction along bladder length l_b (see Fig. B.1). The plane $\hat{\boldsymbol{y}}_f - \hat{\boldsymbol{z}}_f$ is perpendicular to $\hat{\boldsymbol{x}}_f$. Bladder height is h_b and width w_b. We define a small parameter representing slenderness of the fluidic domain $\varepsilon_1 = 2r_c/l \ll 1$, where r_c is the tube radius and $l = l_c\, n_c$ the total length of connective tubing, with l_c the length of a single connective tube and n_c as the total number of connective tubes in a given configuration. Tube and bladder characteristic cross section dimensional scale is $r_c \sim h_b$. The parameters of the fluidic domain are viscosity μ, velocity (u, v, w), gauge pressure p. Under small local strains assumption, bladder cross section area may be expanded to $a(x_f, p, N_e, M_e) = a_0(x_f) + a_{p_1}(p, x_f) + a_{N_1}(N_e, x_f) + a_{M_1}(M_e, x_f)$, where $a_0(x_f)$ is the cross section area of the fluidic domain i.e. bladder-tube array, at the gauge pressure $p = 0$, and $a_{p_1}(p, x_f)$ describes the change of the cross section area due to the fluid pressure, $a_{N_1}(N_e, x_f)$ the change in cross section are due to extensional appendage deformation and $a_{M_1}(M_e, x_f)$ the change in cross section due to appendage bending deformation. The governing equations for the incompressible, creeping, Newtonian flow are the stokes equation,

$$\boldsymbol{\nabla} \mathrm{p} = \mu \nabla^2 \boldsymbol{u} \tag{B.3}$$

and conservation of mass

$$\boldsymbol{\nabla} \cdot \boldsymbol{u} = 0. \tag{B.4}$$

Over the solid domain we use an intrinsic Cosserat rod formulation following Rubin [1,2], limited for the assumption of negligible cross sectional extension, cross sectional shear and tangential

shear respectively limiting the cross section to maintain its initial shape and remain perpendicular the reference curve,

$$m\ddot{\boldsymbol{x}} = m\boldsymbol{b} + [N_{e,3} - \alpha_e V_e]^s \mathbf{e_t} + [V_{e,3} + \alpha_e N_e]^s \mathbf{e_n} + \left[\, \boldsymbol{d}^3 \cdot m\left(\boldsymbol{b}^1 - y^{11}\, \ddot{\boldsymbol{d}}_1\right) \boldsymbol{d}_1 \,\right]_{,3} \tag{B.5}$$

where $\boldsymbol{d}^3 = \boldsymbol{d}_3/d_{33}$ is the reciprocal vector to $\boldsymbol{d}_3$ and the subscript $_{,3}$ stands for the partial derivative with respect to θ. The external distributed force $\boldsymbol{b}$ per unit mass, and external distributed moment per unit mass $\boldsymbol{b}^1$ are defined such,

$$\boldsymbol{b} = \boldsymbol{b}_b + \boldsymbol{b}_c\,, \tag{B.6}$$

$$\boldsymbol{b}^1 = \boldsymbol{b}_b^1 + \boldsymbol{b}_c^1, \tag{B.7}$$

where body force distribution per unit mass $\boldsymbol{b}_b = \left(b_{b_x}[Nm^2/Kg]\,, b_{b_z}[Nm^2/Kg]\right)\rho_s/m$, contact force distribution per unit mass $\boldsymbol{b}_c = \left(b_{c_x}[N/m], b_{c_z}[N/m]\right)/m$, first moment of body force distribution per unit mass $\boldsymbol{b}_b^1 = \frac{\rho_s}{m}\left(b_{b_x}^1[Nm^3/Kg]\,, b_{b_z}^1[Nm^3/Kg]\right)$, first moment of contact force distribution per unit mass $\boldsymbol{b}_c^1 = \frac{1}{m}\left(b_{c_x}^1[Nm/m]\,, b_{c_z}^1[Nm/m]\right)$. We define characteristic appendage deflection $u_1^*[m]$, characteristic first moment of body force distribution per unit mass $b_b^{1*}[Nm/Kg]$, characteristic first moment of contact force distribution per unit mass $b_c^{1*}[Nm/Kg]$, characteristic body force distribution per unit mass $b_b^*[N/Kg]$, characteristic contact force distribution per unit mass $b_c^*[N/Kg]$, characteristic shear force per unit length $b_x^* \sim V_e^*/l_s[N/m]$, characteristic normal force per unit length $b_z^* \sim N_e^*/l_s[N/m]$, characteristic external force per unit mass $b^* \sim b_x^*/m[N/Kg]$, characteristic external moment applied per unit mass $b^{1*} \sim b_x^{1*}/m[Nm/Kg]$, characteristic first moment applied by shear force $(x-axis)$ per unit length $b_x^{1*} \sim b_x^*\, l_s[Nm/m]$, characteristic first moment applied by normal force $(z-axis)$ per unit length $b_z^{1*} \sim b_z^*\, l_s[Nm/m]$. Next, we denote the solid field characteristic appendage extension $u_3^* \sim u_1^*$, characteristic bladder density $\phi^*[bellow/m]$, characteristic elastic-inertial time scale $t_s^*[sec]$, characteristic curvature $\alpha_s^*[1/m]$, characteristic moment resultant $M_e^*[Nm]$, characteristic normal force resultant $N_e^*[N]$, characteristic shear force resultant $V_e^*[N]$ and characteristic squared radius of gyration $y_{11}^* \sim l_s^2[m^2]$. Over the fluid field, we define the characteristic velocity $(u^*, v^*, w^*)[m/sec]$, characteristic gauge pressure $p^*[Pa]$, characteristic fluidic domain cross-section at gage pressure $a_0^*[m^2]$, characteristic change in bladder cross-section $a_1^*[m^2]$ and viscous-elastic time scale $t_f^*[sec]$.

Next we define the normalized variables and coordinates. Normalized appendage curvilinear coordinate $\Theta = \theta/l_s$, inertial-elastic time $T_s = t/t_s^*$, curvilinear deflection axis $X_s = x_s \backslash u_1^*$ and deflection variable $U_1 = u_1/u_1^* = u_1/l_s$, curvilinear extensional axis $Z_s = z_s/l_s$ and extension variable $U_3 = u_3/u_1^*$, appendage curvature $\tilde{\alpha}_s$, appendage stretch $\tilde{\lambda}_s$, moment resultant $\widetilde{M}_e = M_e/M_e^*$, normal force resultant $\widetilde{N}_e = N_e/N_e^*$, shear force resultant $\widetilde{V}_e = V_e/V_e^*$. First moment of body force distribution per unit mass $\boldsymbol{B}_b^1 = \left(b_{b_x}^1/(\frac{b_x^{1^*} l_s^2}{m}), b_{b_z}^1/(\frac{b_z^{1^*} l_s^2}{m})\right)$, first moment of contact force distribution per unit mass $\boldsymbol{B}_c^1 = \left(b_{c_x}^1/b_x^{1^*}, b_{c_z}^1/b_z^{1^*}\right)$, body force distribution per unit mass $\boldsymbol{B}_b = \left(b_{b_x}/(\frac{b_x^* l_s^2}{m})\,, b_{b_z}/(\frac{b_z^* l_s^2}{m})\right)$, contact force distribution per unit mass $\boldsymbol{B}_c = \left(b_{c_x}/b_x^*\,, b_{c_z}/b_z^*\right)$. Fluidic domain spatial coordinates $\left(X_f, Y_f, Z_f\right) = \left(x_f/l,\ y_f/h_b,\ z_f/h_b\right)$, viscous-elastic time $T = t/t_f^*$, fluid velocity $(U,V,W) = (u/u^*,\ v/v^*,\ w/w^*)$, fluid field pressure $P = p/p^* = p/E$, bladder effective fluid pressure for slope generation $P' = p'/E$, bladder effective fluid pressure for extension generation $\bar{P} = \bar{p}/E$, volume flow rate in fluidic cross section $Q = q/(u^* a_0^*)$, bladder permeability $Q_1^b = q_1^b/\tilde{C}^b r_{eff}^4$ and connective tubes' permeability $Q_1^c = q_1^c/\tilde{C}^c r_{eff}^4$, where r_{eff} and $\tilde{C}^i \sim 4\pi$ are respective effective scale and dimensionless constant related to the configuration of the flow-path i.e. shape of the cross-

section, and q_1^i $(i = c, b)$ is defined by the relation $q = -((1/\mu)\partial p/\partial x_f)q_1^i$. Fluidic cross section area is defined $a(x_f, p, N_e, M_e) = a_0(x_f) + a_{p_1}(p, x_f) + a_{N_1}(N_e, x_f) + a_{M_1}(M_e, x_f)$ and is normalized though $a_0^* = \pi r_c^2$ and $a_1^* = (\partial a_1/\partial p)p^*$ such that it reads $A(X_f, P, N_e, M_e) = A_0(X_f) + A_{p_1}(P, X_f)\sigma_p + A_{N_1}(N_e, X_f)\sigma_p + A_{M_1}(M_e, X_f)\sigma_p$ where $\sigma_p = a_1^*/a_0^*$. The slope introduced by a single bladder resulting from fluidic pressure and external traction are $\tilde{\alpha}_p = \alpha_p/\alpha_p^*$ and $\tilde{\alpha}_e = \alpha_e/\alpha_e^*$ respectively, extension introduced by a single bladder resulting from fluidic pressure and external traction are $\tilde{\lambda}_p = \lambda_p/\lambda_p^*$ and $\tilde{\lambda}_e = \lambda_e/\lambda_e^*$ respectively, non-dimensional squared gyration radius is $Y^{11} = y^{11}/y^{11*} = ((\rho_s/m)If_i)/l_s^2$ and last bladder density along appendage length $\Phi = \phi/\phi^* = \phi/((n/2)/l_s)$.

B.3. Analysis

B.3.1. Fluidic Field Governing Equations

Substituting the normalized variables into (1.1) and (B.4) yields in leading order,

$$\frac{\partial P}{\partial X_f} \sim \frac{\partial^2 U}{\partial {Y_f}^2} + \frac{\partial^2 U}{\partial {Z_f}^2}, \qquad \frac{\partial P}{\partial Y_f} \sim 0, \qquad \frac{\partial P}{\partial Z_f} \sim 0, \tag{B.8}$$

$$\frac{\partial U}{\partial X_f} + \frac{\partial V}{\partial Y_f} + \frac{\partial W}{\partial Z_f} \sim 0, \tag{B.9}$$

where $2r_c/l \sim v^*/u^* = \varepsilon_1 \ll 1$ and $u^* = p^*\varepsilon_1^2 l/\mu$. Integrating (B.9) over the fluidic domain cross-section in the $Y_f - Z_f$ plane and applying Gauss theorem yields,

$$\frac{\partial Q}{\partial X_f} + \frac{h}{t_f^* v^*}\frac{\partial A}{\partial T} = 0. \tag{B.10}$$

We define $Q_1\left(A(X_f, P)\right)$ as the normalized volume flow rate calculated by the solution of the Possion equation (B.8) for $\partial P/\partial X_f = -1$ with no-slip boundary condition set at the wall, $(U, V, W) = \boldsymbol{V}_{wall}$. From linearity, Q can be obtained via Q_1 as

$$Q = -\frac{\partial P}{\partial X_f} Q_1\left(A(X_f, P)\right). \tag{B.11}$$

From order-of-magnitude analysis we obtain

$$q_1^{i*} = \tilde{C}^i r_{eff}^4, \qquad i = c, b \tag{B.12}$$

where r_{eff} and $\tilde{C}^i \sim 4\pi$ are respectively the effective scale and dimensionless constant related to the configuration of the flow-path. Taking the derivative of $A(X_f, P, N_e, M_e) = A_0(X_f) + A_{p_1}(P, X_f)\sigma_p + A_{N_1}(N_e, X_f)\sigma_p + A_{M_1}(M_e, X_f)\sigma_p$ with regard to T and substituting (B.11) into (B.10) we obtain,

$$-\left(\frac{\partial^2 P}{\partial {X_f}^2}\cdot Q_1\left(A\left(X_f,P\right)\right)+\frac{\partial P}{\partial X_f}\cdot\left(\frac{\partial Q_1}{\partial X_f}\right)\right)$$
$$+\left(\frac{\partial A_{p_1}(P,\Theta)}{\partial P}\frac{\partial P}{\partial T}+\mathrm{R}\left(X_f\right)\frac{\partial A_{M_1}\left(\widetilde{M}_{\mathrm{e}},\Theta\right)}{\partial \widetilde{M}_e}\frac{\partial \widetilde{M}_e(\Theta,T)}{\partial T}\right. \tag{B.13}$$
$$\left.+\left|\left(\mathrm{R}\left(X_f\right)\right)\right|\frac{\partial A_{N_1}\left(\widetilde{N}_{\mathrm{e}},\Theta\right)}{\partial \widetilde{N}_e}\frac{\partial \widetilde{N}_e(\Theta,T)}{\partial T}\right)=0.$$

The resulting non-linear diffusion equation represents the balance between the change in axial flux to the change of cross section area over time due to fluidic pressure, solid domain section moment resultant and normal force resultant. We define $R\left(X_f\right)=1$ and $R\left(X_f\right)=-1$ discretely to indicate bladder position at the upper or lower row respectively. $\partial A_{M_1}/\partial \widetilde{M}_e$ represents the change in cross section due to section moment resultant and $\partial A_{N_1}/\partial \widetilde{N}_e$ for the change in cross section due to section normal force resultant. From order-of-magnitude analysis of (B.13) we obtain the viscous-elastic time scale t_f^* as,

$$t_f^*=\frac{\sigma_r\mu}{p^*\varepsilon_1^2}=\frac{a_1^*\mu}{a_0^*p^*\varepsilon_1^2}. \tag{B.14}$$

For the case of small local strains of the fluidic cross section due to pressure, and for any bladder geometry, a proportional relation between A_1 and P is upheld, and the viscous elastic time scale becomes $t_f^*=\mu(\partial a_1/\partial p)|_{p=p_0}/a_0^*\varepsilon_1^2$. This proportional relation of $\partial a_{p_1}/\partial p$ is supported over a wide range of pressures as seen in the experimental derivation of system parameters, see SI Appendix C.2 Fig. C.1.

To complete the fluid field model, Equation (B.13) requires us to define two boundary conditions and one initial condition. At $X_f=0$ a Diriclet condition is set representing the pressure input introduced by the syringe pump,

$$P(0,T)=P_{\max}-\Delta P_{max}/\left(1+e^{\left(-2\kappa\left(T-0.5/t_f^*\right)\right)}\right)$$
$$+\Delta P_{max}/\left(1+e^{\left(-2\kappa\left(T-4/t_f^*\right)\right)}\right), \tag{B.15}$$

a Neumann condition at $X_f=1$ representing the last bladder being sealed,

$$\left.\frac{\partial P\left(X_f,T\right)}{\partial X_f}\right|_{X_f=1}=0\,, \tag{B.16}$$

and finally, with the fluid field starting from rest, we set the systems initial condition to

$$P\left(X_f,0\right)=0\,. \tag{B.17}$$

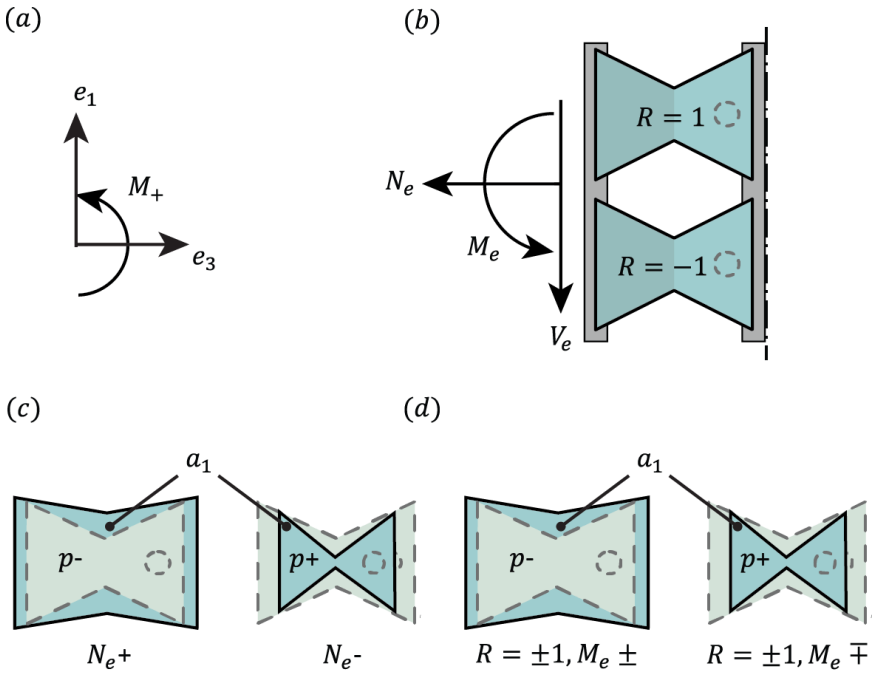

FIG. B.2. ***Illustration of Sign convention using right-handed system.*** *(a) Lab-frame and positive moment defined. (b) Illustration of section internal/resultant forces and moment V_e, N_e, M_e. Bladder change in cross section a_1 presented in response to section resultants: (c) N_e and (d) M_e. Bladder section initial area a_0, is denoted in dashed lines, gray areas indicate induced change in cross section a_1 due to respective resultant.*

B.3.2. Constitutive Laws for a Fluid-Driven Soft Appendage

We now turn formulate the solid field Cosserat rod continuum constitutive laws. Our intrinsic kinematic variables $\lambda_s[1] = \lambda_e + \lambda_p$ stands for the total stretch measure and $\alpha_s[1/m] = \alpha_e + \alpha_p$ for the total curvature measure of the reference curve. The subscript e and p represent the source of the measure being from traction i.e. external forces applied to the surface, or pressure respectively. We define in dimensional form,

Inrinsic Kinematic Variables

$$\lambda_s = \frac{{}^s d_{33}^{1/2}}{{}^s D_{33}^{1/2}}, \tag{B.18}$$

$$\alpha_s = \frac{{}^s \boldsymbol{d}_{1,3} \cdot {}^s \boldsymbol{d}_3}{{}^s d_{33}^{1/2} {}^s D_{33}^{1/2}}, \tag{B.19}$$

where $d_{33} = \boldsymbol{d}_3 \cdot \boldsymbol{d}_3$ defines the metric's of $\boldsymbol{d}_3$ vector at present configuration i.e. spatial frame, and $D_{33} = \boldsymbol{D}_3 \cdot \boldsymbol{D}_3$ defining the metric's of $\boldsymbol{d}_3$ vector at $t = 0$ configuration i.e. material frame. For a beam (straight rod) at relaxed state oriented along the lab frame results in $(\boldsymbol{D}_1, \boldsymbol{D}_2, \boldsymbol{D}_3) = (\boldsymbol{e}_1, \boldsymbol{e}_2, \boldsymbol{e}_3)$, thus we can formulate

$$D_{33} = \boldsymbol{D}_3 \cdot \boldsymbol{D}_3 = \boldsymbol{e}_3 \cdot \boldsymbol{e}_3 = (0,0,1) \cdot (0,0,1) = 1. \tag{B.20}$$

The pressure induced measures for stretch and curvature are defined

$$\lambda_p = \frac{\bar{p}}{E} \frac{\partial \lambda_p}{\partial (\bar{p}/E)}, \tag{B.21}$$

$$\alpha_p = -\frac{p'}{E} \cdot \frac{\partial \alpha_p}{\partial (p'/E)} \tag{B.22}$$

where the effective pressure for slope and extension generation are respectively $p' = (p_d - p_u)$ and $\bar{p} = (p_d + p_u)$. p_u and p_d are the fluidic pressures at the upper and lower bladders, $\partial\lambda_p/\partial(\bar{p}/E)$ is the measure of stretch per cross section per normalized pressure sum and $\partial\alpha_p/\partial(p/E)$ is the measure of curvature per cross section per normalized pressure difference. Formulating the respective non-dimensional form yields

$$\frac{\partial\tilde{\alpha}_p}{\partial(p'/E)} \approx \Phi\frac{\partial\psi}{\partial(p'/E)}, \tag{B.23}$$

$$\frac{\partial\tilde{\lambda}_p}{\partial(\bar{p}/E)} = \Phi\frac{\partial\tilde{\zeta}}{\partial(\bar{p}/E)} \tag{B.24}$$

where $\partial\psi/\partial(p'/E)$ represents the change in appendage slope per cross section per normalized pressure difference and $\partial\tilde{\zeta}/\partial(\bar{p}/E)$ is the non-dimensional change in length per cross section per normalized pressure sum. The later $\partial\tilde{\zeta}/\partial(\bar{p}/E)$ may now be formulated in dimensional in form

$$\frac{\partial\tilde{\zeta}}{\partial(\bar{p}/E)} = \phi^*\frac{\partial\zeta}{\partial(\bar{p}/E)} \tag{B.25}$$

where $\partial\zeta/\partial(\bar{p}/E)$ is the dimensional change in length per cross section per normalized pressure sum.

Substituting our normalized variables into equations (B.1), (B.2) and (B.18) - (B.22) respectively, we obtain our directors and kinematic variables in non-dimensional form,

$$\tilde{\boldsymbol{d}}_1 = \left(\left(\frac{l_s}{u_1^*}\right) + \frac{\partial U_3}{\partial\Theta}, -\frac{\partial U_1}{\partial\Theta}\right), \tag{B.26}$$

$$\tilde{\boldsymbol{d}}_3 = \left(\frac{\partial U_1}{\partial\Theta}, \left(\frac{l_s}{u_1^*}\right) + \frac{\partial U_3}{\partial\Theta}\right) \tag{B.27}$$

and,

$$\tilde{\lambda}_e = \frac{1}{\lambda_e^*}\underbrace{\frac{{}^s\tilde{d}_{33}^{1/2}}{{}^s\tilde{D}_{33}^{1/2}}}_{\tilde{\lambda}_s} - \underbrace{\frac{\lambda_p^*}{\lambda_e^*}\bar{P}(X_f)\frac{\partial\tilde{\lambda}_p}{\partial(\bar{p}/E)}}_{\tilde{\lambda}_p}, \tag{B.28}$$

$$\tilde{\alpha}_e = \frac{1}{l_s\alpha_e^*}\underbrace{\frac{\tilde{d}_{1x,3}\,\tilde{d}_{3x} + \tilde{d}_{1z,3}\,\tilde{d}_{3z}}{{}^s\tilde{d}_{33}^{1/2}\,{}^s\tilde{D}_{33}^{1/2}}}_{\tilde{\alpha}_s} + \underbrace{\frac{\alpha_p^*}{\alpha_e^*}P'(X_f)\frac{\partial\tilde{\alpha}_p}{\partial(p'/E)}}_{\tilde{\alpha}_p}. \tag{B.29}$$

From Order-of-magnitude analysis of we determine the characteristic scale for the directors $d_1^* \sim u_1^*/l_s$ and $d_3^* = u_1^*/l_s$, as well as for the measure of curvature $\alpha_s^* \sim \alpha_e^* \sim \frac{1}{l_s}$ and stretch $\lambda_s^* \sim \lambda_e^* \sim 1$.

Constitutive Equations, Force and Moment Resultants

The constitutive equations for normal force resultant N_e, shear force resultant V_e and bending moment resultant M_e are now formulated in dimensional form,

$$N_e = Eh_sw_sf_e(\lambda_e - 1)\,, \tag{B.30}$$

$$M_e = E\frac{w_sh_s^3}{12}f_i\cdot\alpha_e\,, \tag{B.31}$$

$$V_e = -{}^sd_{33}^{-1/2}M_{e,3}\,. \tag{B.32}$$

Substituting the normalized variables (B.30)-(B.32) become

$$\tilde{N}_e = \left(\tilde{\lambda}_e - \frac{1}{\lambda_e^*}\right), \tag{B.33}$$

$$\tilde{M}_e = \tilde{\alpha}_e\,, \tag{B.34}$$

$$\tilde{V}_e = -\frac{1}{{}^s\tilde{d}_{33}^{1/2}} \frac{\partial \widetilde{M}_e}{\partial \Theta}. \tag{B.35}$$

With order-of-magnitude analysis respectively yielding,

$$N_e^* \sim E h_s w_s f_e \lambda_e^*, \tag{B.36}$$

$$M_e^* \sim E \frac{w_s h_s^3}{12} f_i \frac{1}{l_s}, \tag{B.37}$$

$$V_e^* \sim E \frac{w_s h_s^3}{12} f_i \frac{1}{l_s^2}. \tag{B.38}$$

B.3.3. Serret-Ferent Curvilinear Coordinates

The Serret-Ferent triad associated with the current position along the reference curve is characterized by the unit tangent $^s\boldsymbol{e}_t$ along beam length, the unit normal $^s\boldsymbol{e}_n$ and unit binormal $^s\boldsymbol{e}_\tau$, see illustrated in Fig. B.1. In dimensional form,

$${}^s\mathbf{e_t} = \frac{{}^s\boldsymbol{d}_3(\theta, t)}{{}^s d_{33}^{1/2}}, \tag{B.39}$$

$${}^s\mathbf{e_n} = -\frac{({}^s\boldsymbol{d}_{1,3} \cdot {}^s\boldsymbol{d}_3)^s\boldsymbol{d}_1}{\alpha_s \lambda_s {}^s D_{33}}. \tag{B.40}$$

Substituting the normalized variables yields,

$${}^s\boldsymbol{E_t} = \frac{(\tilde{d}_{3x}, \tilde{d}_{3z})}{{}^s\tilde{d}_{33}^{1/2}}, \tag{B.41}$$

$${}^s\boldsymbol{E_n} = -\frac{(\tilde{d}_{1x}, \tilde{d}_{1z})}{{}^s\tilde{d}_{33}^{\frac{1}{2}}}. \tag{B.42}$$

B.3.4. Solid Field Governing Equations

For the two way coupled solid field governing equations, the intrinsic Cosserat rod formulation is used with both the deflection component U_1 in the $\boldsymbol{e}_1$ lab frame direction and tangential deformation component U_3 in the $\boldsymbol{e}_3$ direction included. Substituting (B.6), (B.7), (B.18) - (B.42) in conjunction with normalized variables and applying order of magnitude analysis onto (B.5) we obtain two scalar equation; one in the X_s direction

$$\begin{aligned} X_s: \Pi_1 \left(\frac{\partial^2 U_1}{\partial T^2} \right) = B_x + \left[\Pi_2 \frac{\partial \widetilde{N}_e}{\partial \Theta} - \Pi_3 \tilde{\alpha}_e \tilde{V}_e \right] {}^s E_{tx} + \left[\Pi_4 \frac{\partial \tilde{V}_e}{\partial \Theta} + \Pi_5 \tilde{\alpha}_e \widetilde{N}_e \right] {}^s E_{nx} \\ + \frac{\partial}{\partial \Theta} \left[\frac{1}{\tilde{d}_{33}} \left(\left(\Pi_6 B_x^1 - \Pi_7 Y^{11} \frac{\partial^2 \tilde{d}_{1x}}{\partial T^2} \right) \tilde{d}_{3x} \right. \right. \\ \left. \left. + \left(\Pi_8 B_z^1 - \Pi_9 Y^{11} \frac{\partial^2 \tilde{d}_{1z}}{\partial T^2} \right) \tilde{d}_{3z} \right) \tilde{d}_{1x} \right] \end{aligned} \tag{B.43}$$

and in the Z_s direction

$$Z_s\colon \Pi_1\left(\frac{\partial^2 U_3}{\partial T^2}\right) = B_z + \left[\Pi_2\,\frac{\partial \tilde{N}_e}{\partial \Theta} - \Pi_3\tilde{\alpha}_e\tilde{V}_e\right]{}^{s}E_{tz} + \left[\Pi_4\frac{\partial \tilde{V}_e}{\partial \Theta} + \Pi_5\tilde{\alpha}_e\tilde{N}_e\right]{}^{s}E_{nz} + \frac{\partial}{\partial \Theta}\left[\frac{1}{\tilde{d}_{33}}\left(\left(\Pi_6 B_x^1 - \Pi_7 Y^{11}\frac{\partial^2 \tilde{d}_{1x}}{\partial T^2}\right)\tilde{d}_{3x} + \left(\Pi_8 B_z^1 - \Pi_9 Y^{11}\frac{\partial^2 \tilde{d}_{1z}}{\partial T^2}\right)\tilde{d}_{3z}\right)\tilde{d}_{1z}\right] \tag{B.44}$$

where both are scaled by non-dimensional numbers $\Pi_1 = \left(t_s^*/t_f^*\right)^2$, $\Pi_2 = N_e^*/(l_s m b^*)$, $\Pi_3 = (\alpha_e^* V_e^*)/(m b^*)$, $\Pi_4 = V_e^*/(l_s m b^*)$, $\Pi_5 = (\alpha_e^* N_e^*)/(m b^*)$, $\Pi_6 = \Pi_8 = (d_1^* b^{1*} d_3^*)/(l_s d_{33}^* b^*)$, $\Pi_7 = \Pi_9 = \left((d_1^* y^{11*} d_3^*)/(l_s^2\, d_{33}^*)\right)\left(t_s^*/t_f^*\right)^2$. These can then be reduced to read,

$$\underbrace{\tau^2\begin{pmatrix}\partial^2 U_1/\partial T^2\\ \partial^2 U_3/\partial T^2\end{pmatrix}}_{Linear\ Inertia} = \underbrace{\begin{pmatrix}B_x\\ B_z\end{pmatrix}}_{Traction} + \underbrace{\left[\eta\,\frac{\partial \tilde{N}_e}{\partial \Theta} - \tilde{\alpha}_e\tilde{V}_e\right]\begin{pmatrix}E_{tx}\\ E_{tz}\end{pmatrix}}_{\substack{Curvelinear\\ Tangential\ force}} + \underbrace{\left[\frac{\partial \tilde{V}_e}{\partial \Theta} + \eta\,\tilde{\alpha}_e\tilde{N}_e\right]\begin{pmatrix}E_{nx}\\ E_{nz}\end{pmatrix}}_{\substack{Curvelinear\\ Normal\ force}} + \underbrace{\frac{\partial}{\partial \Theta}\left[\frac{1}{\tilde{d}_{33}}\begin{pmatrix}\left(B_x^1 - \mathrm{Y}^{11}\tau^2\frac{\partial^2 \tilde{d}_{1x}}{\partial T^2}\right)\tilde{d}_{3x}\\ +\left(B_z^1 - \mathrm{Y}^{11}\tau^2\frac{\partial^2 \tilde{d}_{1z}}{\partial T^2}\right)\tilde{d}_{3z}\end{pmatrix}\begin{pmatrix}\tilde{d}_{1x}\\ \tilde{d}_{1z}\end{pmatrix}\right]}_{Rotary\ Ineria}. \tag{B.45}$$

Where $\tilde{V}_e$ and $\tilde{N}_e$ are the non-dimensional shear and normal force resultants, Θ is the non-dimensional curvilinear length coordinate along the appendage reference curve. We define our kinematic variable for curvature $\tilde{\alpha}_e$, structure reference curve tangent $\boldsymbol{E_t} = \left(\tilde{d}_{3x}, \tilde{d}_{3z}\right)/\tilde{d}_{33}^{1/2}$ and normal $\boldsymbol{E_n} = -\left(\tilde{d}_{1x}, \tilde{d}_{1z}\right)/\tilde{d}_{33}^{1/2}$ components with the non-dimensional directors being $\tilde{\boldsymbol{d}}_1 = (1 + \partial U_3/\partial\Theta, -\partial U_1/\partial\Theta)$ and $\tilde{\boldsymbol{d}}_3 = (\partial U_1/\partial\Theta, 1 + \partial U_3/\partial\Theta)$ and $\tilde{d}_{33} = \tilde{\boldsymbol{d}}_3 \cdot \tilde{\boldsymbol{d}}_3$. Last we define the non-dimensional distributed traction force per unit mass $\boldsymbol{B} = \left(b_x/(V_e^*/l_s m), b_z/(V_e^*/l_s m)\right)$ and moment per unit mass vectors $\boldsymbol{B^1} = \left(b_x^1/(V_e^*/m), b_z^1/(V_e^*/m)\right)$ are respectively. Three nondimensional numbers determining the dynamic regime of the structure. The time scale ratio $\tau = t_s^*/t_f^*$, where $t_s^* \sim \sqrt{m l_s^4/E I f_i}$ is the elastic-inertial time-scale and $t_f^* \sim \mu(\partial a_1/\partial p)|_{p=p_0}/a_0^* \varepsilon_1^2$ the viscous-elastic time scale, the normalized squared radius of gyration $\mathrm{Y}^{11} = I f_i/(w_s h_s f_m l_s^2)$ and the force scale ratio determining the balance between shear and normal forces $\eta = N_e^*/V_e^* = E h_s w_s f_e/\left(E w_s h_s^3 f_i/(12 l_s^2)\right)$. Our force and first moment distribution per unit mass terms are also defined in non-dimensional form, and the respectively defined,

$$\boldsymbol{B} = \left(\frac{\rho_s l_s^2}{m}B_{b_x} + B_{c_x}\ ,\ \frac{\rho_s l_s^2}{m}\left(\frac{b_z^*}{b_x^*}\right)B_{b_z} + \left(\frac{b_z^*}{b_x^*}\right)B_{c_z}\right), \tag{B.46}$$

$$\boldsymbol{B}^1 = \left(\frac{\rho_s l_s^2}{m}B_{b\,x}^1 + B_{c\,x}^1\ ,\ \frac{\rho_s l_s^2}{m}\left(\frac{b_z^{1^*}}{b_x^{1^*}}\right)B_{b\,z}^1 + \left(\frac{b_z^{1^*}}{b_x^{1^*}}\right)B_{c\,z}^1\right). \tag{B.47}$$

Order of magnitude analysis of $\boldsymbol{B}, \boldsymbol{B}^1$ yields $b_x^* \sim V_e^*/l_s$, $b^* \sim b_x^*/m$, $b_x^{1*} \sim b_x^* l_s$, $b^{1*} \sim b_x^{1^*}/m$, $b_z^* \sim N_e^*/l_s$, $b_z^{1*} \sim b_z^* l_s$, $y^{11*} \sim l_s^2$. Determining the relevant dynamic regime of the structure we define the time scale ratio

$$\frac{t_s^*}{t_f^*} = \frac{a_0^* \varepsilon_1^2 \sqrt{m u_1^* l_s^3 / E I f_i}}{\mu (\partial a_1 / \partial p)|_{p=p_0}} \tag{B.48}$$

where $t_s^* \sim \sqrt{m u_1^* l_s^3 / E I f_i}$ is the elastic-inertial time-scale and $t_f^* = \mu (\partial a_1 / \partial p)|_{p=p_0} / a_0^* \varepsilon_1^2$ the viscous-elastic time scale.

For a well-posed problem, Equation (B.45) requires six boundary conditions and four initial conditions. The problem presented in this paper is a cantilever beam. In a similar manner to the classic Euler-Bernoulli beam theory, where boundary conditions are applied over the overall structure quantity of a reference curve, we set the following geometric conditions.

$$U_1(0,T) = 0 \tag{B.49}$$

or slope

$$\left(\frac{\partial U_1}{\partial \Theta}\right)\Big|_{(0,T)} = 0\,, \tag{B.50}$$

and for U_3 extension,

$$U_3(0,T) = 0. \tag{B.51}$$

Dynamic conditions on the other hand, relate to additional displacement due to external moments and normal, shear forces at the boundary. Using (B.29), (B.34) and (B.35), Dynamic conditions are thus applied for moment

$$\widetilde{M}_e\big|_{(1,T)} = 0\,, \tag{B.52}$$

shear force

$$\widetilde{V}_e\big|_{(1,T)} = 0\,, \tag{B.53}$$

and respectively for normal forces over U_3 using (B.33) and (B.28)

$$\widetilde{N}_e\big|_{(1,T)} = 0\,. \tag{B.54}$$

Last, initial conditions are directly applied over U_1 and U_3 setting our appendage to start from rest,

$$U_1(\Theta,0) = 0 \tag{B.55}$$

and

$$U_3(\Theta,0) = 0\,. \tag{B.56}$$

As well as over the initial time derivative,

$$\left(\frac{\partial U_1}{\partial T}\right)\Big|_{(\Theta,0)} = 0 \tag{B.57}$$

and

$$\left(\frac{\partial U_3}{\partial T}\right)\Big|_{(\Theta,0)} = 0\,. \tag{B.58}$$

See Matia & Gat [3] for a more detailed generalized approach for any set of initial and boundary conditions.

B.3.5. Coordinate Mapping Between Solid and Fluid Domains

An essential step in formulating the predictive model is the two-way coordinate mapping of the fluid and solid fields. We thus correlate local pressure gradients associated with the deformation of the structure onto the fluid field to determine deformation-driven flows, and, conversely, we can determine fluid-driven deformation by mapping the distribution of fluid pressure within the structure. Whereas a generalized algorithm for realizing any arbitrary configuration is found in Matia & Gat [3]; In this paper,

we present a simplified approach for configurations with a single continuous array of bladders and tubing across the entire solid field. In Fig. B.3. we present a schematic setup of parallel (panel a) and cross-over (panel b) serpentine configurations discussed in this paper.

We define a methodology for bladder index j from left to right, and separately for top and bottom by $R = 1$ and $R = -1$ respectively see Fig B.3a. **Note:** bladders in the main text are referred to as 'right' and 'left' due robot orientation; these are respective to 'top' and 'bottom' in this appendix.

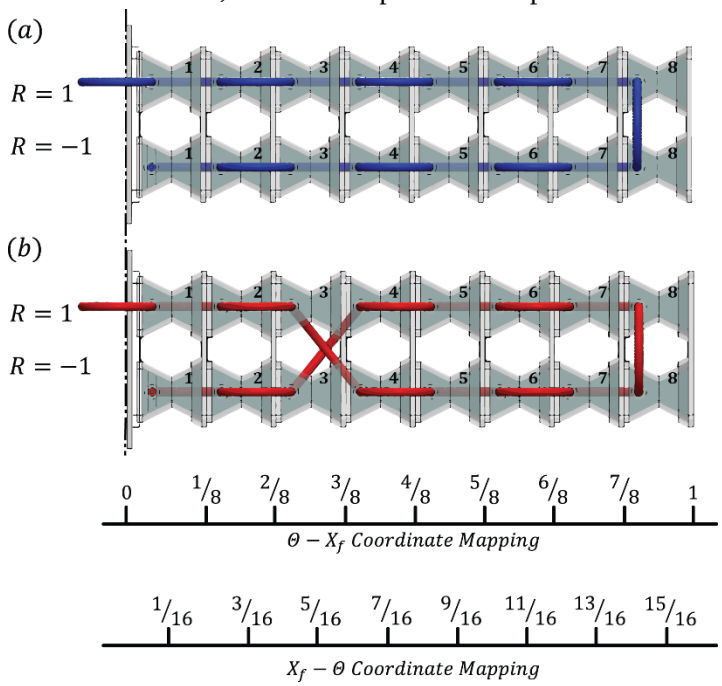

FIG. B.3. ***Schematic illustration of the appendage section showing connectivity configurations.*** *(a) Parallel serpentine configuration. (b) Crossover serpentine configuration. Bladders' index j in black. Scale bars indicate the Θ coordinate used for bladder position in the $\Theta - X_f$ coordinate mapping – bladder start coordinate (upper bar) and $X_f - \Theta$ coordinate mapping – bladder mid coordinate (lower bar).*

$\boldsymbol{\Theta - X_f}$ *Coordinate Mapping,* $\boldsymbol{X_f(\Theta)}$

A mapping of fluid pressure onto the solid field is essential in order to determine the change in stretch and curvature as a result of fluidic pressure gradients. This fluid-driven deformation is introduced by the coupled intrinsic kinematic variables (1.8)(B.28) and (1.9)(B.29), respectively. First, we set the x-axis $(\Theta \cdot R) \in [-1,1]$. $\Theta \in [0,1]$ represents the non-dimensional coordinate along appendage length; the positive or negative signs indicates mapping of the fluid pressure onto a top or bottom bladder respectively, see Fig. B.3. Next, we set the corresponding y-axis X_f. We assign connective array parameters for: number of total bladders $n = 16[1]$ (i.e. for both top and bottom), number of connective tubes $n_c = 15[1]$, length of connective tubes $l_c = 0.04[m]$, length of bladder $l_b = 0.018[m]$; we then calculate the total length of bladder-tube array for mapping purposes $\ell_{tot} = l_b n + l_c n_c$. We define the size of a single bladder along the Θ coordinate as the total non-dimensional length $\Theta = 1$ divided by the number of bladders in one row $|(\Theta \cdot R)| = (1/(\mathrm{n}/2))$. Following, we set the first bladder x-axis coordinate $\Theta^1_{init} = 0$ and end coordinate $\Theta^1_{end} = (1/(\mathrm{n}/2))$. Each consecutive bladder afterwards is given $\Theta^j_{init} = \Theta^{j-1}_{end} + o(1/(\mathrm{n}/2))$ and $\Theta^j_{end} = \Theta^j_{init} + (1/(\mathrm{n}/2))$.

The y-axis is next to be defined. We define the non-dimensional bladder length $\mathcal{L}_b = l_b/\ell_{tot}$ and tube length $\mathcal{L}_c = l_c/\ell_{tot}$, and construct the X_f mapped position such that the solid field coordinate Θ maps to the center of bladder length l_b. The first connecting bladder is set $X_f^1 = \mathcal{L}_b/2$; subsequent connected

bladders are added $X_f^j = X_f^{j-1} + \mathcal{L}_b + \mathcal{L}_c$ in the order of their connection i.e. at the cross over configuration Fig. B.3b the bladder connection order would be $\Omega_c = \{1,2,3,-4,-5,-6,-7,-8,8,7,6,5,4,-3,-2,-1\}$. See Matia & Gat [3] for a more detailed generalized algorithm. The mapping detailed above generates a $\mathcal{C}^0$ continuous mapping function. In Fig. B.4 we plot the coordinate mappings' for parallel serpentine (panel a) and crossover serpentine (panel b). For detailed tabulated data used in the plots, see SI appendix B.4 Table B.1a, B.1b.

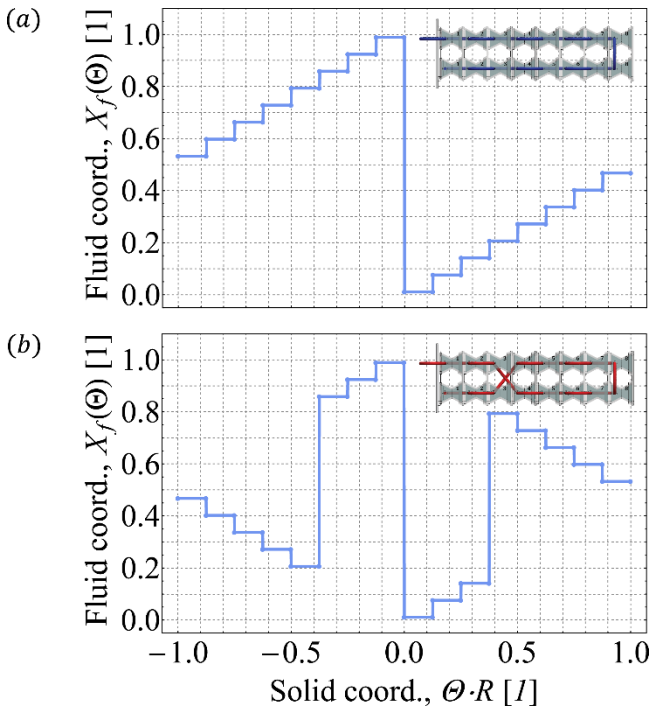

FIG. B.4. ***Plot of coordinate mapping $\Theta - X_f$ for configurations used in the article.*** *(a) Parallel serpentine. (b) Crossover serpentine.*

$X_f - \Theta$ Coordinate Mapping, $\Theta(X_f)$

Next, we turn to map the solid field deformation onto the fluidic pressure field. Equation (1.1) shows deformation as a source term for pressure generation by $\partial\widetilde{M}_e(\Theta,T)/\partial T$ and $\partial\widetilde{N}_e(\Theta,T)/\partial T$.

Our objective is to map our resultants onto the fluid field in order to determine their contribution to it. We set the x-axis to represent the non-dimension length along the fluid domain $X_f \in [0,1]$. As for the y-axis, we prescribe $(\Theta \cdot R) \in [-1,1]$ coordinates corresponding to the solid field mid-bladder lengthwise position $\Theta \in [0,1]$, multiplied by $R = 1$ for the top bladder and $R = -1$ for the bottom bladder.

Following we set mapping. The first connected bladder is assigned an initial $X^1_{f,init} = 0$ and end value $X^1_{f,end} = \mathcal{L}_b$ at its respective $(\Theta \cdot R)$ position. Each subsequent connected bladder is assigned an initial-value $X^j_{f,init} = X^{j-1}_{f,end} + \mathcal{L}_c$ and an end value $X^j_{f,end} = X^j_{f,init} + \mathcal{L}_b$ at respective solid field position $(\Theta \cdot R)$. See Matia & Gat [3] for a more detailed generalized algorithm. The mapping detailed above generates a $\mathcal{C}^0$ continuous mapping function. In Fig. B.5 we present coordinate mappings' for the two configurations considered in this paper: Parallel serpentine (panel a), crossover serpentine (panel b). For detailed tabulated data used in the plots see SI appendix B.5 Table B.2a, B.2b.

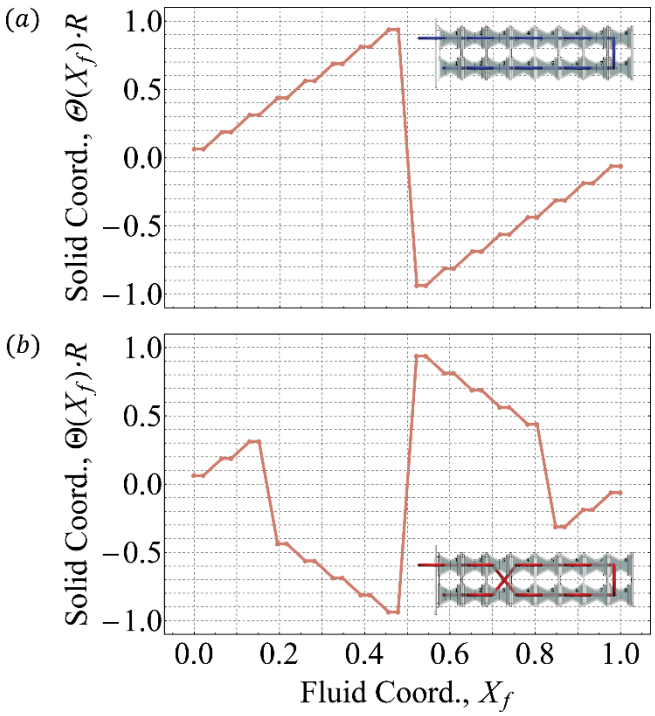

FIG. B.5. ***Plot of coordinate mapping $X_f - \Theta$ for three key configurations used in the article.*** *(a) Parallel serpentine. (b) Crossover serpentine.*

B.3.6. Formulation of $R(X_f)$

The function $R(X_f)$ is a function used to identify the position of a given bladder in an upper or lower row. $R = 1$ indicated an upper bladder and $R = -1$ for lower bladder respectively. It is derived as a $\mathcal{C}^0$ continuous function from the coordinate mapping $X_f - \Theta$ as

$$R(X_f) = \begin{Bmatrix} \Theta(X_f) = 0\,, & 0 \\ \Theta(X_f) \neq 0\,, & \dfrac{\Theta(X_f)}{|\Theta(X_f)|} \end{Bmatrix}. \tag{B.59}$$

B.3.7. Formulation of $\partial A_1/\partial \tilde{N}_e$, $\partial A_1(\tilde{M}_e, \Theta)/\partial \tilde{M}_e$, $\partial A_1(P, \Theta)/\partial P$ and $Q_1\left(A(X_f, P)\right)$

The functions $A_{N_1}(\tilde{N}_e, \Theta)/\partial \tilde{N}_e$, $\partial A_{M_1}(\tilde{M}_e, \Theta)/\partial \tilde{M}_e$, $\partial A_{p_1}(P, \Theta)/\partial P$ represent the change in cross section due to section internal resultants $\tilde{N}_e$, $\tilde{M}_e$ and pressure P. The function $Q_1\left(A(X_f, P)\right)$ stands for the fluidic cross section permeability. The abovementioned functions' value dependents on the fluidic cross section in question being that of a bladder or a connective tube. As such, their value is derived directly from the coordinate mapping $X_f - \Theta$ as a $\mathcal{C}^0$ continuous function differentiating between the parametric value referring to bladder or tube by setting,

$$\Gamma_A(X_f) = \begin{Bmatrix} \dfrac{\partial \Theta(X_f)}{\partial X_f} = 0\,, & 1 \\ \dfrac{\partial \Theta(X_f)}{\partial X_f} \neq 0\,, & 0 \end{Bmatrix}, \tag{B.60}$$

$$\Gamma_Q(X_f) = \begin{cases} \dfrac{\partial \Theta(X_f)}{\partial X_f} = 0\,, & 1 \\ \dfrac{\partial \Theta(X_f)}{\partial X_f} \neq 0\,, & Q_1^c/Q_1^b \end{cases}, \tag{B.61}$$

with bladder permeability Q_1^b and connective tube's Q_1^c respective to X_f position. We can now define the unsteady pressure term representing the change in cross section per unit pressure,

$$\frac{\partial A_{p_1}(P,\Theta)}{\partial P} = \left(\partial A_{p_1}/\partial P\right)\Big|_{p^*} \Gamma_A(X_f)\,, \tag{B.62}$$

and the feedback source terms from the solid field resultants for normal force $\widetilde{N}_e$, and moment $\widetilde{M}_e$ coupling solid field deformation to flow.

$$\frac{\partial A_{N_1}(\widetilde{N}_e,\Theta)}{\partial \widetilde{N}_e} = \left(\partial A_{N_1}/\partial \widetilde{N}_e\right)\big|_{N_e^*}\Gamma_A(X_f)\,, \tag{B.63}$$

$$\frac{\partial A_{M_1}(\widetilde{M}_e,\Theta)}{\partial \widetilde{M}_e} = \left(\partial A_{M_1}/\partial \widetilde{M}_e\right)\big|_{M_e^*}\Gamma_A(X_f)\,, \tag{B.64}$$

For the case of (B.62) - (B.64) the value for $\partial\Theta(X_f)/\partial X_f \neq 0$ is set to zero, as connective tube segments do not change their cross section area due to force and moment resultants (being external to the appendage) nor do they do due to pressure being constant cross section elastic tubes. As such it is of note to mention that for the connective tubes the fluidic governing equation (B.13) degenerates to $\partial^2 P/\partial {X_f}^2 = 0$, lending to the understanding of their contribution to fluid domain pressure solution being a steady state linear pressure gradient proportionate to their length.

And last, we define Q_1 as a function of X_f as we progress from bladder to tube and vice versa along the fluidic domain. Calculating the physical value of q_1^c and q_1^b, see section C.2, we then set our bladder-tube scaling argument for Q_1 using (B.12) separately for a tube $Q_1^c = q_1^c/q_1^{c*}$ and bladder $Q_1^b = q_1^b/q_1^{b*}$ and define

$$Q_1\left(A(X_f,P)\right) = Q_1^b \Gamma_Q(X_f)\,, \tag{B.65}$$

such that we alternate between Q_1^b or Q_1^c respective to X_f position.

B.4. Tabulated Data for $\Theta \rightarrow X_f$ Coordinate Mapping

(a)

$\Theta \cdot R$	$X_f(\Theta)$	$j \cdot R$
−1.000	0.533	−8.
−0.876	0.533	−8.
−0.875	0.598	−7.
−0.751	0.598	−7.
−0.750	0.663	−6.
−0.626	0.663	−6.
−0.625	0.728	−5.
−0.501	0.728	−5.
−0.500	0.793	−4.
−0.376	0.793	−4.
−0.375	0.859	−3.
−0.251	0.859	−3.
−0.250	0.924	−2.
−0.126	0.924	−2.
−0.125	0.989	−1.
−0.001	0.989	−1.
0.000	0.011	1.
0.125	0.011	1.
0.126	0.076	2.
0.250	0.076	2.
0.251	0.141	3.
0.375	0.141	3.
0.376	0.207	4.
0.500	0.207	4.
0.501	0.272	5.
0.625	0.272	5.
0.626	0.337	6.
0.750	0.337	6.
0.751	0.402	7.
0.875	0.402	7.
0.876	0.467	8.
1.000	0.467	8.

(b)

$\Theta \cdot R$	$X_f(\Theta)$	$j \cdot R$
−1.000	0.467	−8.
−0.876	0.467	−8.
−0.875	0.402	−7.
−0.751	0.402	−7.
−0.750	0.337	−6.
−0.626	0.337	−6.
−0.625	0.272	−5.
−0.501	0.272	−5.
−0.500	0.207	−4.
−0.376	0.207	−4.
−0.375	0.859	−3.
−0.251	0.859	−3.
−0.250	0.924	−2.
−0.126	0.924	−2.
−0.125	0.989	−1.
−0.001	0.989	−1.
0.000	0.011	1.
0.125	0.011	1.
0.126	0.076	2.
0.250	0.076	2.
0.251	0.141	3.
0.375	0.141	3.
0.376	0.793	4.
0.500	0.793	4.
0.501	0.728	5.
0.625	0.728	5.
0.626	0.663	6.
0.750	0.663	6.
0.751	0.598	7.
0.875	0.598	7.
0.876	0.533	8.
1.000	0.533	8.

TABLE. B.1. ***Tabulated data for $\Theta \rightarrow X_f$ coordinate mapping used in figure B.4.*** *(a) Parallel serpentine configuration. (b) Crossover serpentine configuration..*

B.5. Tabulated Data for $X_f \rightarrow \Theta$ Coordinate Mapping

(a)

X_f	$\Theta(X_f)$	$j \cdot R$
0.000	0.063	1.
0.022	0.063	1.
0.065	0.188	2.
0.087	0.188	2.
0.130	0.313	3.
0.152	0.313	3.
0.196	0.438	4.
0.217	0.438	4.
0.261	0.563	5.
0.283	0.563	5.
0.326	0.688	6.
0.348	0.688	6.
0.391	0.813	7.
0.413	0.813	7.
0.457	0.938	8.
0.478	0.938	8.
1.000	−0.063	−1.
0.978	−0.063	−1.
0.935	−0.188	−2.
0.913	−0.188	−2.
0.870	−0.313	−3.
0.848	−0.313	−3.
0.804	−0.438	−4.
0.783	−0.438	−4.
0.739	−0.563	−5.
0.717	−0.563	−5.
0.674	−0.688	−6.
0.652	−0.688	−6.
0.609	−0.813	−7.
0.587	−0.813	−7.
0.543	−0.938	−8.
0.522	−0.938	−8.

(b)

X_f	$\Theta(X_f)$	$j \cdot R$
0.000	0.063	1.
0.022	0.063	1.
0.065	0.188	2.
0.087	0.188	2.
0.130	0.313	3.
0.152	0.313	3.
0.804	0.438	4.
0.783	0.438	4.
0.739	0.563	5.
0.717	0.563	5.
0.674	0.688	6.
0.652	0.688	6.
0.609	0.813	7.
0.587	0.813	7.
0.543	0.938	8.
0.522	0.938	8.
1.000	−0.063	−1.
0.978	−0.063	−1.
0.935	−0.188	−2.
0.913	−0.188	−2.
0.870	−0.313	−3.
0.848	−0.313	−3.
0.196	−0.438	−4.
0.217	−0.438	−4.
0.261	−0.563	−5.
0.283	−0.563	−5.
0.326	−0.688	−6.
0.348	−0.688	−6.
0.391	−0.813	−7.
0.413	−0.813	−7.
0.457	−0.938	−8.
0.478	−0.938	−8.

TABLE. B.2. ***Tabulated data for $\mathbf{X_f \rightarrow \Theta}$ coordinate mapping used in figure B.5****. (a) Parallel serpentine configuration. (b) Crossover serpentine configuration.*

Appendix C

This appendix describes the setups used to experimentally measure six model parameters related to internal external pressure, forces, volume, and elastic modulus. Unless otherwise noted all experiments were replicated 10 times with a single 16-bladder actuator mounted at the top, which is also where the pressure inlet/outlet is located. We manually inflated a syringe filled with air. We read the change in the volume of air on the syringe, and recorded pressure using a $20 - 400[kPa]$ absolute pressure sensor 1040_0 from Phidgets. Four markers were placed on alternate links on the actuator, such that the actuator pose in steady state could be automatically extracted from side-view photos using Image.

C.1. Inlet pressure versus Volume

To measure the change in volume given an inlet pressure, we manually inflated a 16-bladder actuator with a crossed configuration, while recording the amount of displaced volume in the syringe and the steady-state pressure (Fig. C.1(A)). Starting at ambient pressure, we added a volume of air in the range of $-60[mL]$ to $+40[mL]$, and repeated each trial 10 times. This range corresponds to that used in the final hexapod robot described in the main article. The data is shown in Fig. C.1(B); note that volume added is reported per bladder in the actuator. We used the slope of this curve to inform the parameter $\partial a_1/\partial P$.

C.2. Differential Inlet Pressure versus Actuator Curvature

To measure the actuator curvature versus the inlet pressure, we connected the 8 bladders on either side to two separate syringes which was inflated opposite of each other (Fig. C.1(C)). We then computed the angle between the last two markers, as seen in Fig. C.1(D). We used the slope of this curve to inform the parameter $\partial\psi/\partial(p'/E)$, where $E = 1.8[MPa]$.

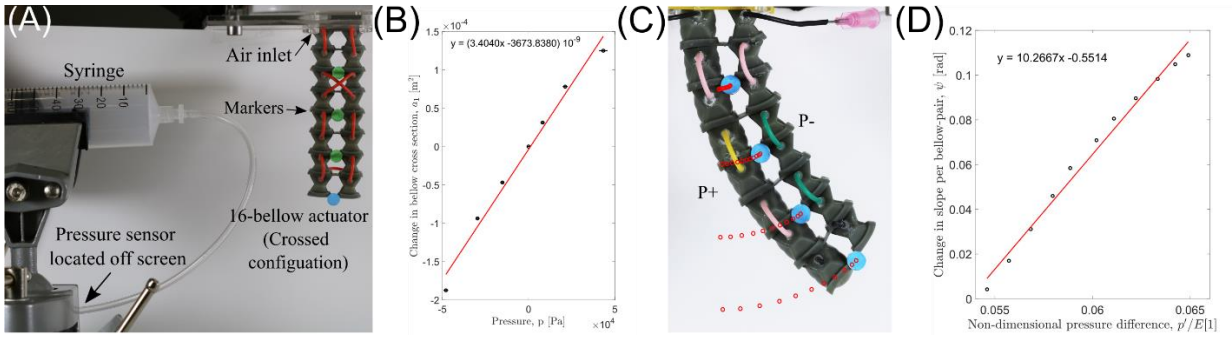

FIG. C.1. (A) Experimental setup to determine pressure versus volume. (B) Data related to (A): mean and standard deviation shown in blue; best fit line in red. (C) Photo of experimental setup, showing the actuator bending towards the side which has negative pressure relative to the other. The overlay of red points show where the four markers were tracked. (D) Data related to (C). The curvature at the tip of the actuator is approximated as the angle of the line through the third to the fourth marker with respect to vertical.

C.3. Inlet Pressure versus Actuator Elongation

To measure the bladder elongation versus applied pressure we manually inflated a 16-bladder actuator in a crossed configuration. The outcome is shown in Fig. C.2(A). The properties of this curve informs the parameter $\partial\zeta/\partial(\bar{p}/E)$, where $E = 1.8[MPa]$.

C.4. Normal Force versus Actuator Extension and Compression

To measure actuator extension under strain, we mounted a cup to the bottom of a 16-bladder actuator connected in a straight configuration and added weight in the range of 0 to $300[g]$ with $20[g]$ intervals. A weight of $300[g]$ roughly correspond to one third the weight of the full hexapod robot, i.e. similar to what the robot would experience when balancing on three actuators. We measured the change in bladder volume, by connecting the actuator such that its in/outlet tube extruded into separate skinny, transparent cylinder partially filled with water. The amount of displaced water corresponds to changes in actuator volume.

To measure actuator compression under a normal force, we flipped it upside down and added a similar range of weight to the top. To keep the actuator from buckling under the normal force, we placed it in a square tube. The data from these two experiments is shown in Fig. C.2(A-B). This curve informs parameter $\partial a_1/\partial N_e$.

C.5. Torque versus Actuator Curvature

To measure bladder curvature under external torque, we connected two bladders, similar to that described in Sec. C.4, such that their in/outlet tube extruded into separate skinny, transparent cylinders partially filled with water. We then created a pulley system with weights in the range 0 to $300[g]$ to create a moment on the bladders, as shown in the inset in Fig. C.2(C), and recorded the amount of air displaced in the cylinders. The outcome is shown in Fig. C.2(C). The properties of this curve informs the parameter $\partial a_1/\partial M_e$.

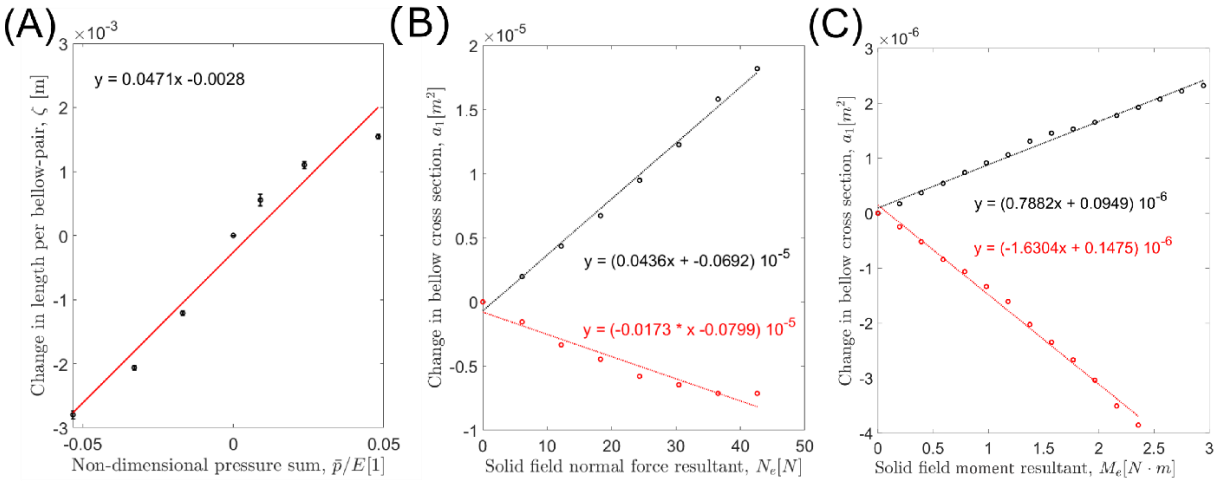

FIG. C.2. (A) bladder elongation versus pressure. Black markers show mean and standard deviation over 10 data points; the red curve is a fitted line. (B) bladder inflation (black) and deflation (red) under extension and compression. Dashed curve and text show fitted lines. (C) Change in bladder volume in response to torque; the inset shows a sketch of the experimental setup..

C.6. Procedural Generation of Gait Inlet Pressure Signal

To generate a motion cycle that takes advantage of the entire range of deformations possible with the experimental system, we formulated four guiding principles based on our time scale analysis to define the parameters of the following input signal function, $p(0,t) = p_{\max} - \Delta p_{max}/\left(1 + e^{\left(-2\kappa\left(t/t_f^* - t_{init}/t_f^*\right)\right)}\right) + \Delta p_{max}/\left(1 + e^{\left(-2\kappa\left(t/t_f^* - t_{end}/t_f^*\right)\right)}\right)$. First, we set the upper work point, $p_{max} \approx 40[kPa]$ from the mid-stroke position, to positively displace fluid to achieve the desired extension from the neutral length l_s (at steady state) while supporting the weight of the robot. Second, we set the lower work point p_{min} from the mid-stroke position so that the negative displacement volume evacuates the entire volume of the actuator (or actuators for the entire robot). Therefore, we ensure that the actuator is firmly buckled during the gait cycle, giving us the maximum lift. We have now also defined $\Delta p_{max} = p_{max} - p_{min} \approx 140[kPa]$. Third, we set the average input time scale $t_i^* = O(t_f^*)$ to $\approx 0.75 - 1 \approx 0.875[sec]$, as the time required by the pump to span Δp_{max} (positive and negative strokes may differ), and derive our sigmoid logistic growth rate $\kappa = (6/\delta_T)$ by the non-dimensional transition period $\delta_T = \langle t_i^*/t_f^* \rangle \approx 6$. Thus, we ensure a maximal pressure gradient between bladders on opposite sides of the actuator's neutral plane, leading to maximal stride length. (4) In the same way as with sigmoid functions, we set the plateau period of the input signal to be proportional to$(t_{init} - t_{end}) \approx 14t_f^*$ which corresponds to the time it takes the fluid to travel the entire length of the connective tubing array l. Using this plateau period as a guide, we can estimate the periodic extension for the gait cycle to be $\approx 42t_f^*$, corresponding to two transition periods and two plateau periods; the gait cycle frequency is, therefore, $\approx 1/42t_f^*$.

Referances

1. Rubin, M. B. *Cosserat Theories: Shells, Rods and Points*. (Springer Science & Business Media, 2013).
2. Rubin, M. B. An intrinsic formulation for nonlinear elastic rods. *International Journal of Solids and Structures* **34**, 4191–4212 (1997).
3. Y. Matia, A. D. Gat, Dynamics of fluid driven autonomous materials: Interconnected fluid filled cavities to realize autonomous materials (2021).